Dalton Transactions

ROYAL SOCIETY OF CHEMISTRY

PAPER

View Article Online
View Journal | View Issue

Open Access Article. Published on 05 April 2023. Downloaded on 6/26/2024 9:07:45 AM.
This article is licensed under a Creative Commons Attribution-NonCommercial 3.0 Unported Licence.

Check for updates

Cite this: *Dalton Trans.*, 2023, **52**, 6360

A new family of luminescent iridium complexes: synthesis, optical, and cytotoxic studies†

Gonzalo Millán,‡[a] Mattia Nieddu,‡[a,b] Icíar P. López,[c] Cintia Ezquerro,[a] Jesús R. Berenguer,[a] Ignacio M. Larráyoz,[d,e] José G. Pichel*[c,f] and Elena Lalinde*[a]

By using *N*,*N*-dibutyl-2,2′-bipyridine-4,4′-dicarboxamide as a diimine (*dbbpy*) and distinctive cyclometalated groups, this work reports a new family of cationic phosphorescent Ir(III) cyclometalated [Ir(C^N)$_2$(N^N)]X compounds [C^N = difluorophenylpyridine (dfppy) **a**, 2,6-difluoro-3-(pyridin-2-yl)benzaldehyde (CHO-dfppy) **b**, and 2,6-difluoro-3-pyridin-2-yl-benzoic acid (COOH-dfppy) **c**; X = Cl$^-$ **2a,b,c-Cl**; X = PF_6^- **2b,c-PF$_6$**]. For comparative purposes, the related complex [Ir(dfppy)$_2$(H$_2$dcbpy)]$^+$ (**3a-PF$_6$**) incorporating 3,3′-dicarboxy-2,2′-bipyridine as an auxiliary ligand (N^N = H$_2$dcbpy) is also presented. All complexes have been fully characterized and their photophysical properties were investigated in detail. The theoretically calculated results obtained by density functional theory (DFT) and time-dependent density functional theory (TD-DFT) studies indicate that luminescence is derived from mixed ^{3}ML′CT (Ir → N^N)/^{3}LL′CT (C^N → N^N) excited states with the predominant metal-to-diimine charge transfer character. Their antineoplastic activity against tumour cell lines A549 (lung carcinoma) and HeLa (cervix carcinoma), as well as the nontumor BEAS-2B (bronchial epithelium) cell line was assessed and fluorescence microscopy studies were performed for their cellular localization. Among them, **2a-Cl** exhibited the most potent anticancer activity, being higher than cisplatin. However, **2b-Cl** and **2c-Cl,-PF$_6$** were the least toxic, while **2b-PF$_6$** and **3a-PF$_6$** exhibited only moderate activity. Confocal microscopy studies for **2a-Cl** suggest that complexes localize preferentially in the lysosomes and to a lesser extent in the cytoplasm, but ultimately causing damage to the mitochondria. Finally, the potential photodynamic behaviour of scarcely toxic complexes **2b-Cl**, **2b-PF$_6$**, **2c-Cl** and **3a-PF$_6$** was also studied.

Received 4th January 2023,
Accepted 4th April 2023

DOI: 10.1039/d3dt00028a

rsc.li/dalton

Introduction

Given their efficacy, platinum-based agents (cisplatin, carboplatin, and oxaliplatin) are amongst the most prescribed chemotherapeutics in oncologic treatments.[1–10] The cytotoxicity of these drugs mainly relies on the formation of intrastrand cross-links with guanine residues, triggering the inhibition of DNA transcription and apoptosis of cancer cells.[11,12] However, despite their effectiveness in cancer chemotherapy, their poor selectivity and the acquired resistance of some tumours together with the lack of effective approaches in the treatment of aggressive metastatic cancers force the development of new drugs. To this end, the design of new cisplatin-like or Pt(IV) derivatives and prodrugs to target specific receptors or tumour cells,[13] including new delivery systems to reduce side effects,[14,15] is a very active area that has been recently reviewed. Moreover, in recent decades, the search for nonplatinum metal-based drugs capable of combining high anticancer activity, low cytotoxicity and a mechanism of action that differs from those of the cisplatin family has increased exponentially.[16–22] In this context, many transition metals have been tested as antineoplastic agents.[19,23] In addition, the incorporation of new strategies, such as thermo-, chemo- and photodynamic[24] therapies, and also synergistic treatments as a combination of several modalities to treat cancer are providing

[a]*Departamento de Química-Centro de Síntesis Química de La Rioja, (CISQ), Universidad de La Rioja, 26006 Logroño, Spain. E-mail: elena.lalinde@unirioja.es*
[b]*Chair of Biogenic Functional Materials, Technical University of Munich, Schulgasse, 22, Straubing 94315, Germany*
[c]*Lung Cancer and Respiratory Diseases Unit (CIBIR), Fundación Rioja Salud, 26006 Logroño, Spain. E-mail: jgpichel@riojasalud.es*
[d]*Unidad Predepartamental de Enfermería, Universidad de La Rioja, Duquesa de la Victoria 88, E–26006 Logroño, Spain. E-mail: ignacio.larrayoz@unirioja.es*
[e]*Biomarkers and Molecular Signaling Unit (CIBIR), Fundación Rioja Salud, 26006 Logroño, Spain*
[f]*Biomedical Research Networking Center in Respiratory Diseases (CIBERES), ISCIII, Spain*

†Electronic supplementary information (ESI) available: Experimental section, tables and figures giving structural, spectroscopic, photophysical, and theoretical data, and biological studies for the compounds. CCDC 2231729 and 2231730. For ESI and crystallographic data in CIF or other electronic format see DOI: https://doi.org/10.1039/d3dt00028a

‡These authors have contributed equally to this work.

This journal is © The Royal Society of Chemistry 2023

Open Access Article. Published on 05 April 2023. Downloaded on 6/26/2024 9:07:45 AM. This article is licensed under a Creative Commons Attribution-NonCommercial 3.0 Unported Licence.

excellent antitumor effects. In particular, photodynamic therapy (PDT) is an emerging cancer treatment strategy that shows fewer side effects and higher selectivity than conventional therapies. It involves the excitation of a non-toxic photosensitizer (PS) with light to produce a long-lasting triplet excited state that can interact with oxygen ($^3O_2$) to produce reactive oxygen species (ROS) through type I (electron transfer) or type II (energy transfer) mechanisms. Singlet oxygen that is generated *via* the type II mechanism has been implicated as the most important mediator of the anticancer effects of PDT. ROS are produced in a wide range of physiological processes, particularly by mitochondria. Nevertheless, uncontrolled and excessive production of ROS, or a decreased ability of cells to scavenge ROS, gives rise to oxidative stress and subsequent damage to various cellular components, causing apoptosis and cell necrosis.[25,26]

In this field, organometallic iridium complexes are an attractive class of compounds that have demonstrated great potential as an alternative to platinum-based metallodrugs.[27] Iridium complexes have demonstrated promising antiproliferative activity *in vitro* and/or *in vivo* through various mechanisms of action, such as disturbance of cellular redox homeostasis, interaction with proteins, or regulation of non-apoptotic pathways.[28–32] Moreover, due to their exceptional photophysical properties and good cell permeability, phosphorescent cyclometalated iridium(III) complexes have been tested in cellular imaging as biomolecular probes,[33–35] anticancer drugs, and photosensitizers (PSs) to produce singlet oxygen ($^1O_2$).[26,36] As cyclometalated iridium complexes integrate the anticancer efficacy and excellent phosphorescence properties, they have shown great potential as theranostic agents.[26,34,35,37] In particular, cationic cyclometalated iridium (III) complexes with ancillary diimine ligands $[Ir(C^N)_2(N^N)]^+$ stand out in this field because they display rich emissive-state characteristics, which include high quantum yields, large Stokes shifts, long-lasting luminescence, and good photostability, which can be tuned depending on the C^N backbone and the diimine ligand. Commonly, the ^{3}MLCT, ligand-to-ligand charge-transfer (^{3}LLCT), and intraligand (^{3}IL) excited states compete for the emission depending on the energy levels of frontier orbitals. Moreover, together with their cationic nature, proper incorporation of substituents on the cyclometalated group or the diimine ligand could result in the modification of their cell permeability and their physio-chemical and biological activities.[38–40]

Here, we report a new family of cationic Ir(III) cyclometalated $[Ir(C^N)_2(N^N)]^+$ compounds with *N*,*N*-dibutyl-2,2′-bipyridine-4,4′-dicarboxamide as the diimine (*dbbpy*) and different cyclometalated backbones (**2a–c**) [C^N = difluorophenylpyridine (dfppy) **a**, 2,6-difluoro-3-(pyridin-2-yl) benzaldehyde (CHO-dfppy) **b**, and 2,6-difluoro-3-pyridin-2-yl-benzoic acid (COOH-dfppy) **c**]. Due to the low solubility of **2b-Cl** and **2c-Cl**, the related **2b-PF$_6$** and **2c-PF$_6$** complexes were prepared using PF_6^- as the counter anion. For comparison, the complex $[Ir(dfppy)_2(H_2dcbpy)]^+$ (**3a-PF$_6$**; H_2dcbpy = 3,3′-dicarboxy-2,2′-bipyridine) is also included. It is remarkable that complexes bearing an acid in the cyclometalated group show increased solubility, even in water.[41] Their optical properties supported by theoretical calculations are presented. Their antineoplastic activity against tumour cell lines A549 (lung carcinoma) and HeLa (cervix carcinoma) as well as the nontumor BEAS-2B (bronchial epithelium) cell lines was assessed and fluorescence microscopy studies for their cellular localization were performed. Finally, the potential photodynamic properties of the scarcely toxic complexes **2b-Cl**, **2b-PF$_6$**, **2c-Cl** and **3a-PF$_6$** were also evaluated.

Results and discussion

Synthesis and characterization

The HC^N compounds 2,6-difluoro-3-(pyridin-2-yl) benzaldehyde (CHO-dfppyH)[42] and 2,6-difluoro-3-pyridin-2-yl-benzoic acid (COOH-dfppyH),[43] and the diimine *N*,*N*′-dibutyl-2,2′-bipyridine-4,4′-dicarboxamide (*dbbpy*)[44] have been previously reported. The new organometallic chloride-bridged diiridium precursors $[Ir(CHO\text{-}dfppy)_2(\mu\text{-}Cl)]_2$ (**1b**) and $[Ir(COOH\text{-}dfppy)_2(\mu\text{-}Cl)]_2$ (**1c**) were synthesized following similar procedures to those previously established for $[Ir(dfppy)_2(\mu\text{-}Cl)]_2$ (**1a**).[45] The mononuclear complexes **2-Cl** were prepared by refluxing a mixture of the chelating ligand *dbbpy* and the corresponding iridium precursor (**1**) in MeOH/CH_2Cl_2 for 12 h (Scheme 1). Analogous complexes with PF_6 as the counter anion (**2b-PF$_6$** and **2c-PF$_6$**) could be prepared as pure complexes following a procedure described by Zhou *et al.*,[46] instead of anion exchange reactions starting from **2-Cl** derivatives. This procedure involves the *in situ* formation of the solvated acetonitrile complexes $[Ir(CHO\text{-}dfppy)_2(NCMe)_2]PF_6$ and $[Ir(COOH\text{-}dfppy)_2(MeCN)_2]$, respectively, and the subsequent treatment with the *dbbpy* ligand (Scheme 1), avoiding the presence of mixed counterions in the reaction media. Finally, the synthesis of $[Ir(dfppy)_2(H_2dcbpy)]PF_6$ (**3a-PF$_6$**) was carried out following a similar procedure to that reported by Amouri, Barbieri *et al.*[47] for related complexes with the 4,4′-dicarboxy-2,2′-bipyridine ligand (see the ESI† for details).

All of the products have been characterized using high-resolution mass spectrometry and different spectroscopic means (IR and multinuclear ^{1}H, $^{13}C\{^1H\}$, and ^{19}F NMR spectra and ^1H–^1H COSY, ^1H–^{13}C HMBC, HSQC correlation experiments; see the ESI,† Experimental section). The ESI mass spectra of complexes **2** and **3a-PF$_6$** confirmed the presence of the molecular peak $[M]^+$ with the expected isotopic distribution, while the precursor complexes **1b** and **1c** showed peaks at *m*/*z* 665.02 (100%) and 702.06 (100%) corresponding to the bridge splitting $[Ir(CHO\text{-}dfppy)_2Cl + H]^+$ and $[Ir(COOH\text{-}dfppy)_2 + Na + H_2O]^+$ species, respectively. The FTIR spectra of complexes **2** and **3a-PF$_6$** exhibit characteristic vibration bands of C=O (1660 cm^{-1}) and N–H of amide groups (only for **2**, 3350–3250 cm^{-1}), and the complexes with PF_6 show an intense band at 800 cm^{-1}. The NMR images of the binuclear iridium complexes in $CDCl_3$ for **1b** and in D_2O/KOH mixture for **1c** show the presence of

Open Access Article. Published on 05 April 2023. Downloaded on 6/26/2024 9:07:45 AM.
This article is licensed under a Creative Commons Attribution-NonCommercial 3.0 Unported Licence.

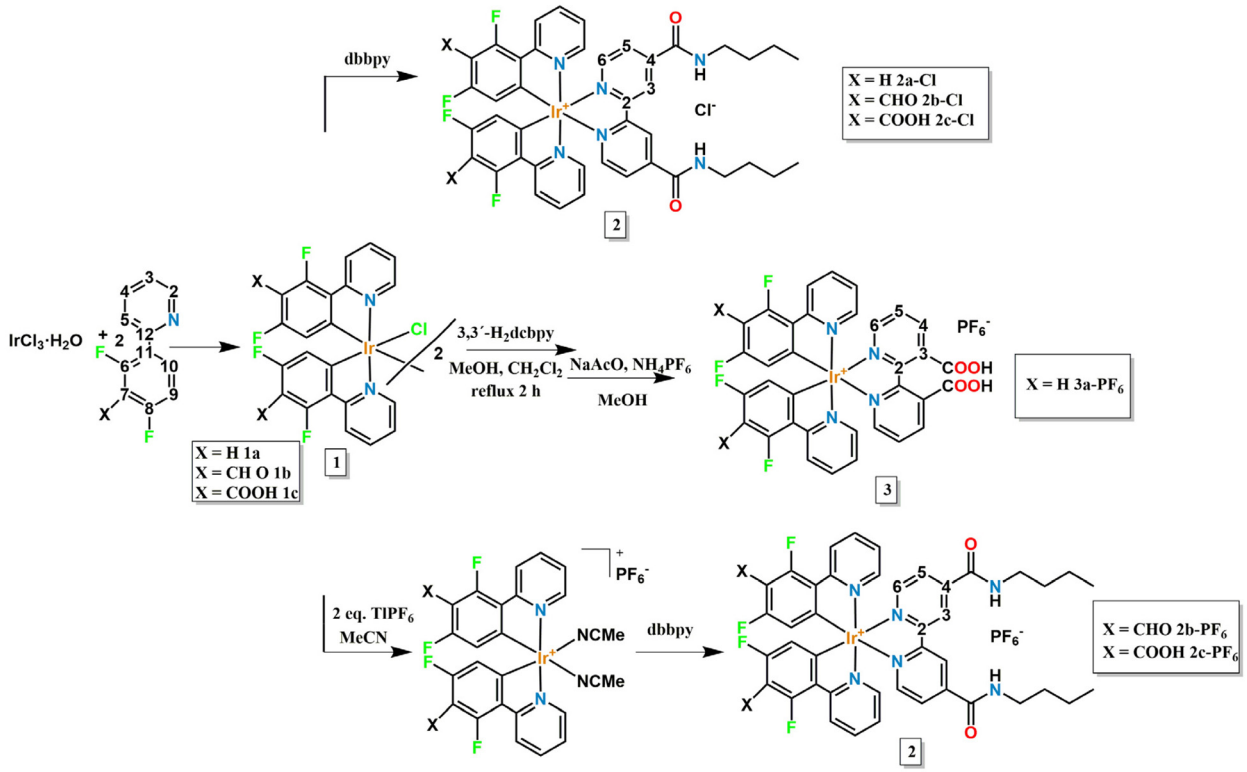

Scheme 1 Synthesis of compounds **1**, **2(a–c)** and **3a-PF_6**.

only one type of chemically equivalent cyclometalated ligands, as expected for the formation of a single isomer (two isomers are possible, a meso form and a racemic pair). However, in DMSO solution two sets of cyclometalated ligands are generated, indicating the cleavage of the chloride bridging system in the presence of the highly coordinating DMSO, to form [Ir(CHO-dfppy)$_2$Cl(DMSO)] (**1b-DMSO**) (Fig. S.1.1†) and [Ir(COOH-dfppy)$_2$Cl(DMSO)] (**1c-DMSO**), respectively. This behaviour is not unusual and has been reported before.[48–50] The ^{1}H and ^{13}C{^{1}H} NMR spectra ($CDCl_3$ for **2a,b**, MeOD for **2c-Cl**, and acetone-d_6 **2c-PF_6**, **3a-PF_6**; see the ESI†) showed the presence of the expected signals for a C_2 symmetry with the two cyclometalated group equivalents and a symmetrical bipyridine ligand. In complexes **2**, featuring the *dbbpy* ligand, the singlet corresponding to the H^3 protons, adjacent to the amide function, appeared as the most deshielded signal (~10.6 **2a,b-Cl**, 9.2 **2c-Cl**, 10.30 **2b-PF_6**, 9.21 **2c-PF_6**); however, the amide CONH occurred as a broad resonance, which is slightly downfield shifted in complexes **2-Cl** relative to **2-PF_6** (9.63 **2a-Cl**, 9.53 **2b-Cl** *vs.* 9.36 **2b-PF_6**, 8.34 **2c-PF_6**), likely due to the interaction with Cl^- (CONH···Cl···HNCO), as observed by X-ray diffraction in the solid state. In **2c-Cl**, this resonance is lost, likely due to a fast exchange with MeOD. The ^{13}C{^{1}H} and ^{19}F NMR spectra also confirmed the formation of the complexes. Thus, two doublet signals for the non-equivalent F^6 and F^8 fluorine resonances are seen in all complexes, with the additional expected doublet due to PF_6^- in complexes with this counter anion. Furthermore, the structures of complex **2a-Cl** and **[2c]$^+$** were determined by X-ray diffraction.

Single yellow crystals of **2a-Cl** were obtained by diffusion of *n*-hexane into a saturated solution of the corresponding complex in CH_2Cl_2 at room temperature. However, slow diffusion of *n*-heptane into a solution of complex **2c-PF_6** in acetone afforded yellow crystals that were identified as **2c-PO_2F_2–acetone** due to partial hydrolysis of the counter anion. Both complexes crystallized in the $P_{21/n}$ space group and, as expected for centrosymmetric space groups, both enantiomers (Δ and Λ) are present in the lattice. A view of the cationic part with selected bond lengths and angles are presented in Fig. 1 and Table S1.† Both cations exhibited the characteristic octahedral environment around the Ir^{III} center, with a mutual *cis*-disposition of C-metalated and a *trans* arrangement of the corresponding nitrogen atoms of the 2-(2,4-difluorophenyl)pyridine cyclometalated ligands. The bond distances and angles were comparable to those found in analogous compounds.[25,51,52] In both anions, the Ir–C distances were within the expected values (~2.01 Å). The Ir–N2 distances to the *dbbpy* ligand (~2.13 Å) were longer than the corresponding Ir–N1 (~2.05 Å, C^N) distance, in accordance with the strong trans influence of the metalated C atom. The chelating C–Ir–$N_{(C^N)}$ angles are around 80° while the N–Ir–$N_{(C^N)}$ were roughly 174.5°, similar to those observed in related complexes. A close look into the structures revealed the presence of hydrogen bonding interactions. Thus, in complex **2a-Cl**, short hydro-

 This journal is © The Royal Society of Chemistry 2023

Open Access Article. Published on 05 April 2023. Downloaded on 6/26/2024 9:07:45 AM.
This article is licensed under a Creative Commons Attribution-NonCommercial 3.0 Unported Licence.

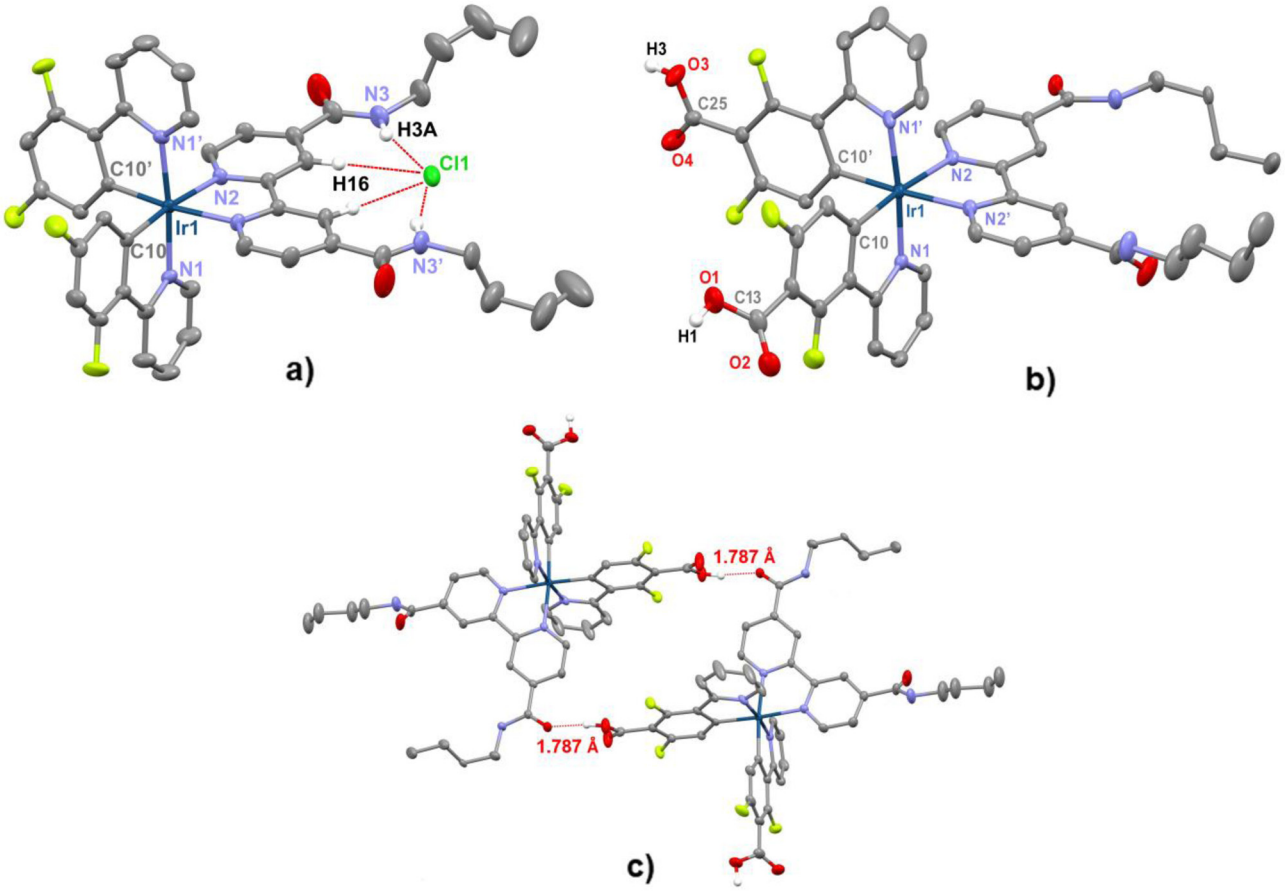

Fig. 1 (a) Molecular structure of complex [Ir(dfppy)$_2$(dbbpy)]Cl (**2a-Cl**), (b) view of the cation [Ir(COOH-dfppy)$_2$(dbbpy)]$^+$ (from structure of **2c-PO$_2$F$_2$**), and (c) view of the dimer formed by two cations **[2c]$^+$** through hydrogen bonds between the ketonic group of one amide and the carboxylic group of one cyclometalated ligand. Selected bond distances (Å) and angles (°); **2a-Cl**: Ir(1)–C(10) 2.008(2), Ir(1)–N(1) 2.049(2), Ir(1)–N(2) 2.125(2), Cl(1)···H(16) 2.601(1), Cl(1)···H(3A) 2.458(1). N(1)–Ir(1)–C(10) 80.46(8), N(1)–Ir(1)–C(10′) 95.73(8), N(2)–Ir(1)–N(2′) 77.3(1), N(1)–Ir(1)–N(1′) 174.63(9). **[2c]$^+$**: Ir(1)–C(10) 2.009(4), Ir(1)–N(1) 2.042(3), Ir(1)–N(2) 2.131(3). N(1)–Ir(1)–C(10) 80.5(1), N(1′)–Ir(1)–C(10) 97.3(1), N(2)–Ir(1)–N(2′) 76.7(1), N(1)–Ir(1)–N(1′) 174.6(1).

gen bonding between the Cl$^-$ anion and the H atoms of the two carboxyamide groups (CONH) is observed (Cl···H3–N 2.458 (1) Å). Furthermore, Cl is also close to the adjacent H atom of the pyridine rings (Cl···H–C(16) 2.601(1) Å). These distances, which were shorter than the sum of van der Waals radii (2.95 Å), are comparable to those reported in other complexes,[53–58] thus supporting the formation of an ionic pair in which the chloride acts as an acceptor of four hydrogen donors of the chelating *dbbpy* ligand. In its turn, in the crystal of **2c-PO$_2$F$_2$** the cations dimerize through short hydrogen bonding between the ketonic group of one of the carboxyamide arms and the carboxylic group of the cyclometalated ligand. The O···H distance (1.79 Å) and the angle O···H–O (164.9) are comparable to those seen in other systems.[59]

Noncovalent interactions (NCI analysis) have been carried out on the ionic pair **2a-Cl.** The interactions were colour coded with blue and green colours, indicating strong and moderate attractive forces, respectively, while the red and yellow ones correspond to strong and weak repulsive forces (Fig. 2). In the NCI plot, clear green surfaces between the NH and CH protons of *dbbpy* ligand and chloride atom developed, thus supporting the involvement of donor–acceptor interactions between the anion Cl and the H–X (X = N, C). In addition, green surfaces were also observed for intramolecular C–X···π (dfppy) (X = F, H).

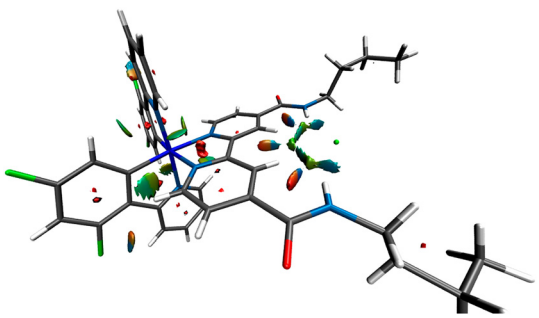

Fig. 2 NCI plot isosurfaces of the noncovalent interactions of **2a-Cl** generated for *s* = 0.3.

Open Access Article. Published on 05 April 2023. Downloaded on 6/26/2024 9:07:45 AM.
This article is licensed under a Creative Commons Attribution-NonCommercial 3.0 Unported Licence.

Photophysical properties and theoretical calculations

Absorption spectra. The UV–vis absorption spectra of all compounds were recorded in dimethyl sulfoxide, and the corresponding data are given in Table 1. Selected spectra for **2-Cl** and **3a-PF$_6$** are shown in Fig. 3. The counter anion for complexes **2** has negligible influence on their maxima. For complexes **2-Cl**, the absorption spectra were also recorded in different solvents showing minor variations in their maxima (Table S7 and Fig. S10†). Moreover, concentration dependence studies in DMSO (1×10^{-6} to 1×10^{-2} M) have been carried out for complexes **2-Cl**, showing that the three complexes follow the Beer–Lambert Law and, thus, no remarkable ground-state aggregation phenomena occur in solution (Fig. S11†).

According to TD-DFT calculations on complexes **2-Cl** (see the ESI†), the intense high energy absorption features in the UV region (<350 nm) are ascribed to spin allowed π–π* transitions of the ligands (^{1}IL C^N, L′ *dbbpy*) with metal to ligand contribution (MLCT and ML′CT). In mononuclear complexes **2**, the moderately intense band around 365 nm can be mainly related to the intense S_3 transition, which is associated with H-1 to the LUMO. H-1 resides on the cyclometalated ligands (91–92%) and Ir (7%) while the LUMO is located on the *dbbpy* ligand. Therefore, this band mainly arises from spin allowed ^{1}LL′CT (C^N → *dbbpy*) transitions with some ^{1}ML′CT contribution. The low energy band extending in the region of $\lambda >$ 400 nm (447 **2a-Cl**, 421 **2b-Cl**, 409 nm **2c-Cl**) is associated with the HOMO → LUMO transitions, having an ML′CT/LL′CT character. The slightly hypsochromic shift on going from **2a-Cl** to **2c-Cl** is reflected in the calculations (S_1, cal. 472 **2a-Cl**, 427 **2b-Cl**; 410 nm **2c**), and can be attributed to the stabilization of the HOMO due to the presence of the electron withdrawing CHO and COOH substituents (Fig. 4). Due to strong spin–orbit coupling (SOC) associated with iridium, an overlapping with the spin-forbidden singlet–triplet metal-to-ligand and ligand-to-ligand transitions (^{3}ML′CT/^{3}LL′CT) is expected in this region. In complex **3a-PF$_6$**, having the dicarboxy-pyridine (3,3′ H_2dcbpy), the low energy feature appears at *ca.* 450 nm with a tail extending to 500 nm, also with an ML′CT/LL′CT character according to calculations (see the ESI†).

Table 1 Absorption data in DMSO solution (5×10^{-5} M) of complexes **1–3**

Complex	λ_{abs}/nm (ε/×10^{-3}/M^{-1} cm^{-1}) DMSO
1b-DMSO	293 (29.96), 333 (9.72), 366 (5.58)
1c-DMSO	277 (60.2), 292 (52.4), 365 (9.6)
2a-Cl	273 (62.6), 310 (33.8), 368 (9.5), 447 (1.3), 469 (0.7)
2b-Cl	306 (23.8), 328 (13.7), 358 (4.4), 421 (1.1)
2b-PF$_6$	276 (43.2), 305 (32.5), 332 (19.4), 358 (7.8), 421 (1.0)
2c-Cl	269 (54.2), 284 (60.4), 300 (52.4), 365 (9.6), 409 (1.4)
2c-PF$_6$	281 (51.4), 300 (34.2), 363 (8.6), 431 (2.4)
3a-PF$_6$	265 (41.8), 305$_h$ (20.94), 361 (6.48), 450 (0.93)

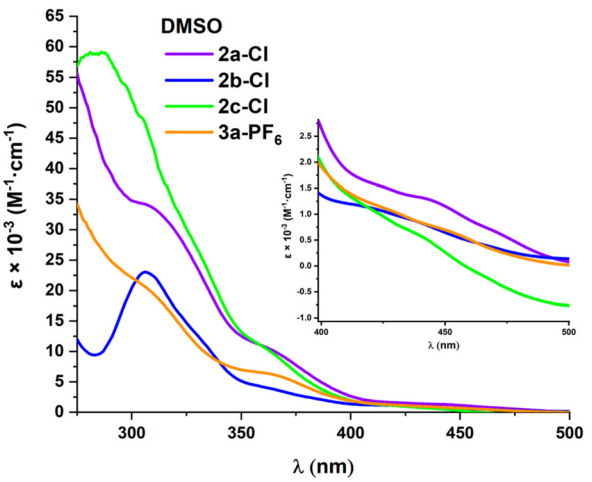

Fig. 3 Absorption spectra of complexes **2-Cl** and **3a-PF$_6$** in DMSO solution (5×10^{-5} M) at 298 K. Inset: expansion of the low energy region (400–500 nm).

Emission spectra. The room temperature emission spectra of the precursor complex **1c** and complexes **2** and **3** were recorded in DMSO solution (Fig. 5) and in the solid state (Fig. S12†) and the data are listed in Table 2 and Table S8.† For complexes **2-Cl**, the spectra were also examined in different solvents aiming to check the solvatochromic behaviour, which is common in this type of complexes (Fig. S13†). As an example, the emission spectra in DMSO solution are shown in Fig. 5a. The precursor complex **1c** was highly soluble in DMSO and, as noted before, generated the solvate **1c-DMSO** upon dissolution, which exhibits a slightly structured band located at 511 nm which is ascribed to a ^{3}LC with a ^{3}MLCT character (Fig. 5b). In the solid state the emission of **1c** was red shifted to 580 nm, suggesting that the emission might have originated from molecular aggregation of the dinuclear derivative in the rigid media through ππ stacking of the cyclometalated ligands. A highest energy shoulder is observed at 540 nm that is likely due to the emission from the ^{3}MLCT/^{3}LC contribution on individual molecules (Fig. S13†). In DMSO solution, the complexes **2-Cl** and **2-PF$_6$** were brightly emissive and exhibited similar photophysical properties. All complexes displayed broad unstructured bands in the range of 540–565 nm, with a negligible influence of the counter anion likely due to the easy breakdown of the hydrogen bonding interactions in complexes **2-Cl**. In agreement with theoretical calculations and previous works,[58,60,61] this emission is attributed to a mixed ^{3}ML′CT (Ir → N^N)/^{3}LL′CT (C^N → N^N) excited state with a predominant ML′CT character. The photoluminescence quantum yields (PLQYs) in deaerated solutions (ϕ) were relatively high (from 44.6% for **2b-PF$_6$** to 54.1 for **2c-PF$_6$**), with lifetimes in the range 0.58 to 0.81 μs. As expected, compared with the deoxygenated atmosphere, the emission intensity under an air atmosphere was notably reduced. In the case of complex **3a-PF$_6$**, the emission is red shifted (λ_{max} = 605 nm) and the photoluminescence quantum yield drops to 4.2%, as does the decay to 0.31 μs. This result is not unexpected and is in accordance with the energy gap law. The measured lower lifetime of complexes **2** (0.58–081 μs) and **3a-PF$_6$** (0.31 μs) measured in deoxygenated solutions in relation to **1c** can be attributed to a notable higher metal contribution

This journal is © The Royal Society of Chemistry 2023

Open Access Article. Published on 05 April 2023. Downloaded on 6/26/2024 9:07:45 AM.
This article is licensed under a Creative Commons Attribution-NonCommercial 3.0 Unported Licence.

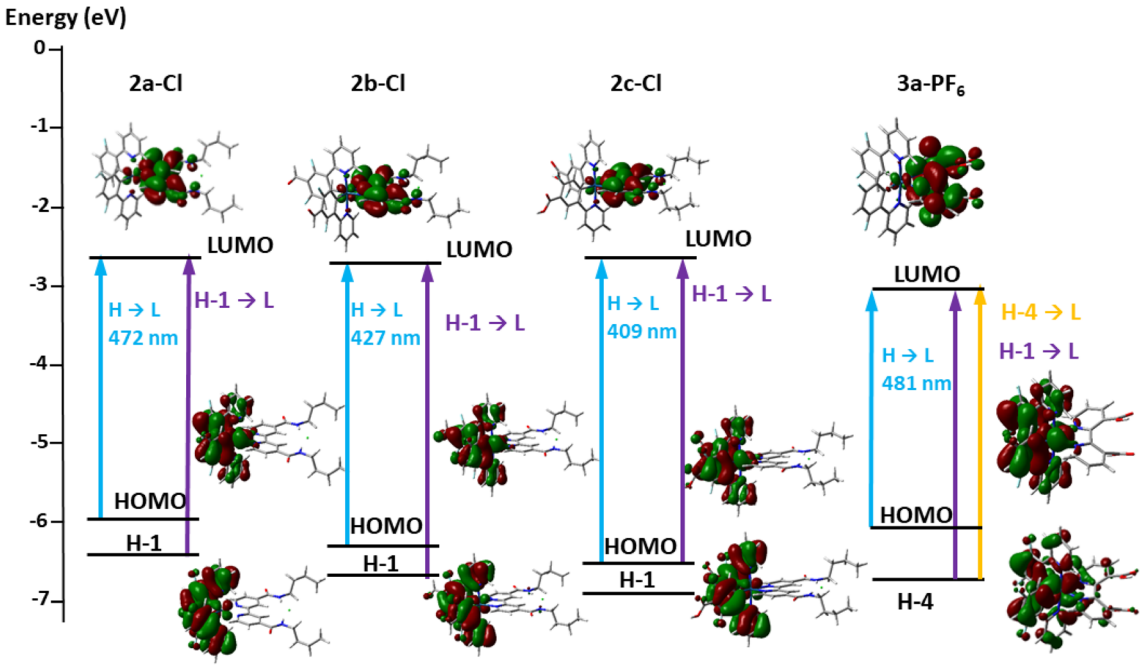

Fig. 4 Schematic representation of selected excitation for complexes **2-Cl** and **3a-PF$_6$** in DMSO.

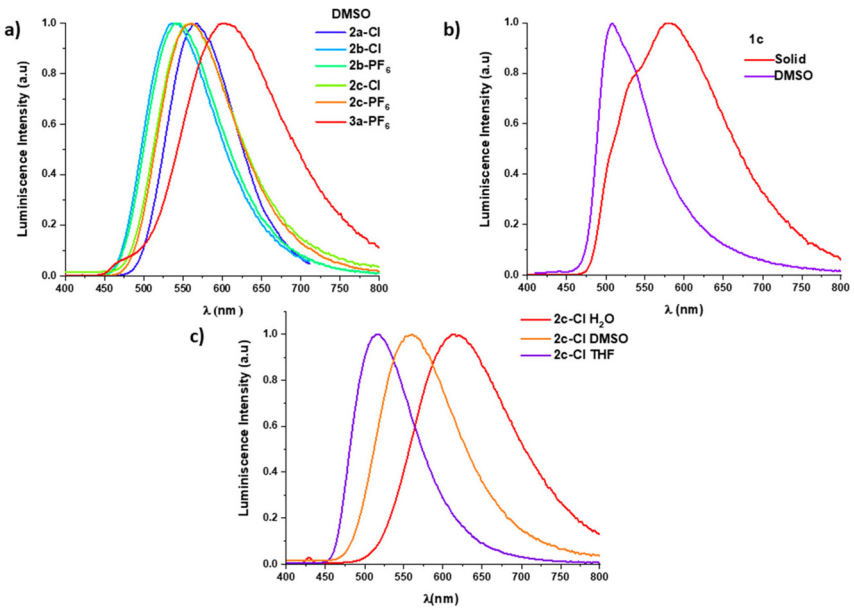

Fig. 5 Normalized emission spectra of complexes (a) complexes **2**–**3** in DMSO solution (5 × 10^{-4} M), (b) **1c** in different media, and (c) of complex **2c-Cl** in different solvents.

in the excited state. Comparing the complexes with the *dbbpy* ligand, the emission maxima follow the order (540 **2b** < 560 **2c** < 565 **2a**), which is consistent with the stabilization of the HOMO in complexes featuring the CHO and COOH substituents. In complex **3a-PF$_6$**, the observed red shift can be attributed to a remarkable stabilization of the target 3,3′-H$_2$dcbpy LUMO (Fig. 4 and 5a). The reduced quantum yield of this complex (Table 2), which is reflected in the higher k_{nr} and lower k_r in relation to complexes **2**, could be related to the relatively strong vibrational quenching effect caused by the presence of the two carboxylic units on the bipyridine ligand.

The influence of the solvent has been examined for complexes **2-Cl** (see Fig. 5c, and Table S8 and Fig. S13 in the ESI† for **2c-Cl**). For these complexes, the emission band gradually shifts hypsochromically as the solvent polarity decreases (**2a-Cl** 565 DMSO, 520 THF and 495 nm toluene; **2b-Cl** 540 DMSO,

Open Access Article. Published on 05 April 2023. Downloaded on 6/26/2024 9:07:45 AM.
This article is licensed under a Creative Commons Attribution-NonCommercial 3.0 Unported Licence.

Table 2 Photophysical data in DMSO solution (5×10^{-4} M)[a]. Radiative (K_r) and non-radiative (K_{nr}) constants calculated at room temperature

Complex	λ_{em} (nm)	Energy/λ_{em} [a]	τ (μs) aereated/ deoxygenated	φ aereated/ deoxygenated	K_r [b]/s^{-1}	K_{nr} [b]/s^{-1}
1c	510	—	10.14[b]	—/<0.01	$1.5 \times \cdot 10^3$	9.7×10^4
2a-Cl	568	2.2 eV/556	0.18/0.81	0.15/0.53	6.6×10^5	5.7×10^5
2b-Cl	540	2.5 eV/494	0.42/0.72	0.35/0.51	7.1×10^5	6.8×10^5
2b-PF_6	542	—	0.28/0.58	0.21/0.45	7.7×10^5	9.6×10^5
2c-Cl	558	2.4 eV/510	0.43/0.76	—/0.54	7.1×10^5	6.1×10^5
2c-PF_6	558	—	0.41/0.73	0.25/0.54	7.4×10^5	6.3×10^5
3a-PF_6	605	1.7 eV/715	0.14/0.31	0.02/0.04	1.4×10^5	3.1×10^6

[a] Predicted from DFT (B3LYP/LANL2DZ (Ir) 31G(d,p)) calculations in DMSO at 298 K, by estimating the energy difference between the optimized T_1 and singlet state S_0. [b] Values from deoxygenated solution.

507 THF and 503 nm toluene; **2c-Cl** 615 H_2O, 540 DMSO, and 517 nm THF). The observed positive solvatochromism indicates that the excited state is more polar than the ground state, being stabilized by the solvent polarity and confirms the strong charge transfer nature of the excited state. For **2a-Cl**, the decay and the PLQY decrease with the polarity of the solvent. This feature is very remarkable for complex **2c-Cl**, featuring the COOHdfppy cyclometalated ligand, in H_2O wherein the PLQY falls to 3.1% with a decay of 0.06 μs. In this complex, the exchange of carboxylic and H_2O protons opens a new channel for deactivation, as reflected in the high value for k_{nr} (1.7×10^{-7} s^{-1}).

To ascertain the detailed properties of the excited state, the optimized geometries of T_1 have been calculated using the S_0 geometries and the B3LYP approach for complexes **2a–c-Cl** and **3a-PF_6**. Fig. 6 shows the optimized excited-state structures of the highest singly occupied molecular orbitals (HSOMOs), lowest singly occupied molecular orbitals (LSOMOs), and spin density distributions. In all complexes, the SOMO-1 involves Ir metal and the C^N cyclometalating group, while the SOMO is primarily localized on the bipyridine. The predicted spin densities have been localized over the bipyridine ligand and, thus, the emissions are mainly characterized by both ML′CT from iridium to bipyridine charge transfer and LL′CT from the cyclometalated to the bipyridine ligand. There is good agreement between the experimental and calculated emission wavelengths shown in Table 2 (calculated by estimating the energy difference between the optimized T_1 and singlet state S_0 in DMSO). The introduction of CHO (**2b**) and COOH (**2c**) substituents on the cyclometalated group caused a slight hypsochromic shift by the stabilization of the SOMO-1 in relation to **2a-Cl**, while the incorporation of carboxylic units on the bipyridine provoked a remarkable bathochromic shift, which is in good agreement with the experimental data.

Quantum yield $^1O_2$ quantification. In photodynamic therapy, the presence of singlet oxygen is one of the most

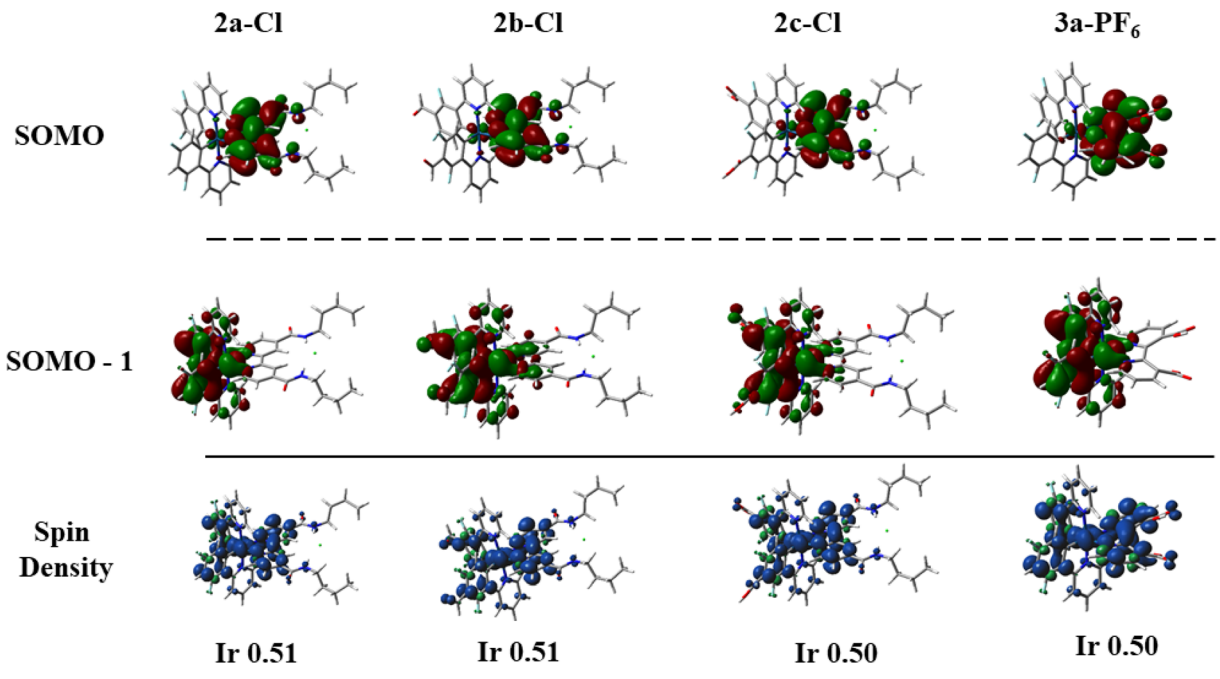

Fig. 6 Calculated SOMO, SOMO-1 and spin density representations of **2** (**a**, **b** and **c**)-**Cl** and **3a-PF_6** in DMSO solution.

This journal is © The Royal Society of Chemistry 2023

Open Access Article. Published on 05 April 2023. Downloaded on 6/26/2024 9:07:45 AM.
This article is licensed under a Creative Commons Attribution-NonCommercial 3.0 Unported Licence.

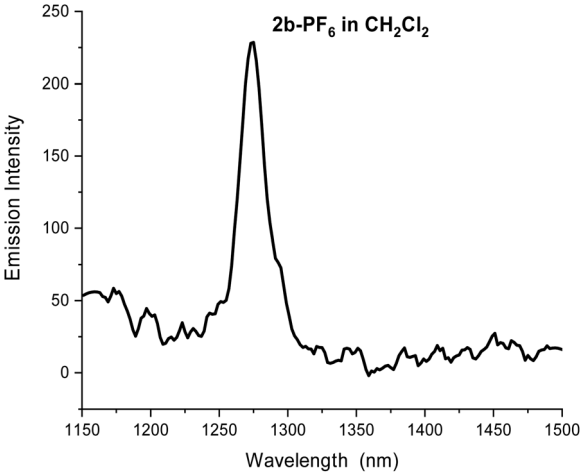

Fig. 7 Emission band of the singlet oxygen from fresh solution of **2b-PF$_6$** (λ_{ex} 425 nm).

important factors for the enhancement of the cytotoxic activity of a complex. Therefore, complexes **2b-Cl**, **2b-PF$_6$**, **2c-Cl** and **3a-PF$_6$** were selected to assess their ability to generate $^1O_2$. These complexes generate singlet oxygen ($^1O_2$) at room temperature in CH_2Cl_2 solution (Fig. 7). The $^1O_2$ oxygen emission at 1270 nm was directly monitored using a near-infrared detector upon excitation at 425 nm. To determine the singlet oxygen generation, we use a reference method by UV-Visible spectroscopy in acetonitrile. ROS generation was visualized using the common ROS-capturing agent 1,3-disphenylisobenzofuran (DPBF). DPBF reacts with ROS to generate 1,2-dibenzoylbenzene, resulting in an absorbance decline at 410 nm.[62,63] The activity of a mixture of each complex with DPBF in acetonitrile solution, employing $[Ru(bpy)_3]_2$ as a reference (φ_Δ^S = 0.56),[64] was measured under blue light irradiation (λ 460 nm). A clear decrease in the absorbance of the DPBF band at 410 nm (Fig. S14†) demonstrated the generation of $^1O_2$ by the Ir(III) complexes. The values of φ obtained for all four complexes (0.32 for **2b-PF$_6$**, 0.12 for **2c-Cl**, 0.10 for **3a-PF$_6$**, and 0.09 for **2b-Cl**) suggest that they might have future potential as an intracellular $^1O_2$ generator for photo-chemotherapeutic development.

Biological studies

To start, the stability of complexes **2** and **3a** was supported by ^{1}H NMR or UV-Vis spectra in DMSO solution or cellular medium, respectively, which revealed that they remained unaltered within 74 h (Fig. S15–S18 and S20†). Their photostability in both media was also assessed. The complexes were found to be stable upon blue light irradiation with a blue lamp (396 nm) for at least 10 min (Fig. S19 for **3a-PF$_6$** and S21† for **2b,c-Cl** and **3a-PF$_6$**). The cytotoxicity of complexes **2** and **3a** was determined *in vitro* against human cell lines by an MTS-based method. We also evaluated the effect of irradiation with UV light on the antiproliferative activity of complexes **2b** (**Cl** and **PF$_6$**), **2c-Cl** and **3a-PF$_6$**, their interaction with DNA and lipophilicity, as well as their cellular localization.

Cytotoxic activity and selectivity index. The IC_{50} values were determined against two different human tumours (A549, lung carcinoma and HeLa, cervix carcinoma) and nontumoral BEAS-2B (bronchial epithelium) cell lines after cellular exposure to the compounds for 72 h and compared to cisplatin as reference (Table 3 and Fig. S22†).

Complexes **2b-Cl** and **2c-Cl** compounds displayed IC_{50} values ≥100 μM towards the A549 cell line (Fig. S22†). The low toxicity found with this assay could be attributed to their low solubility in the aqueous biological media. For that reason, the related complexes with PF_6^- as the counter anion were prepared to test their biological activity. Complexes **2-PF$_6$** displayed better solubility, with no signs of precipitation at concentrations up to 100 μM. For **2c-PF$_6$**, the IC_{50} value was also ≥100 μM towards the A549 cell line (Fig. S22†). Based on the low cytotoxicity of **2b-Cl**, **2c-Cl** and **2c-PF$_6$**, these complexes were not further analysed in other cells. However, it is remarkable that the antiproliferative activity improved on going from **2b-Cl** to **2b-PF$_6$** (IC_{50} values of 27.17 and 74.60 in A549 and HeLa cells, respectively, for **2b-PF$_6$** *vs*. the lesser effects of **2b-Cl**). This change might be attributed to the close interactions between Cl^- anion and the two NH groups of the butylamide substituents of the dbbpy ligand in compound **2b-Cl**, which decreases its ionic character and solubility, thus preventing their optimum cellular uptake. Interestingly, complex **2a-Cl**, offered the lower IC_{50} values, being even more cytotoxic than cisplatin in both A549 (3.73 *vs*. 6.45) and HeLa (5.53 *vs*. 13.60) cells (Table 3). These values are similar to those reported for related complexes $[Ir(C\hat{}N)_2(N\hat{}N)]PF_6$ (C^N = ppy, dfppy) featuring as diimine the dibutyl 2,2′-bipyridine-4,4′-dicarboxylate against HeLa and A549 tumour cells (IC_{50} 1.7–2.3).[69] Complex **3a-PF$_6$** that contains two carboxylic acid units on the diimine ligand also showed mild cytotoxic activity, with IC_{50} values similar to **2b-PF$_6$** (32.87 and 51.22 in A549 and HeLa cells, respectively) (Table 3 and Fig. S22†). As a rule, all the complexes were more active towards the A549 cell line rather than HeLa, in accordance with our previous results.[62,66]

In order to evaluate the selectivity index (SI) of complexes towards the tumour cell lines, we used normal epithelial lung virus-transformed BEAS-2B cells as a non-tumor reference cell line. Cisplatin IC_{50} value towards this cell line was 1.74 μM, slightly lower than those for A549 and HeLa cells, therefore rendering low SI values of this anti-cancer drug for these cell lines (0.27 and 0.13, respectively) (Table 3). Actually, compounds with SI values of <2 are assumed to give general toxicity.[70,71] IC_{50} values of cisplatin on BEAS-2B cells and their SI values for A549 and HeLa cells reported here are in good agreement with previous findings.[72–74] Among the Ir(III) complexes, the better values of the selectivity index (SI) were given by complex **2a-Cl** in both tumoral A549 (3.30) and HeLa (2.23) cells, due to its higher cytotoxic activity in these cells (IC_{50} 3.73 and 5.53 in A549 and HeLa cells, respectively) compared to that in non-tumoral BEAS-2B cells (IC_{50} 12.32 μM). SI values for complex **2b-PF$_6$** and **3a-PF$_6$** were 1.90 and 0.73 (A549) and 0.69 and 0.47 (HeLa), respectively (Table 3), indicating low selective toxicity towards cancer cells. Low SI values (<2) for

Open Access Article. Published on 05 April 2023. Downloaded on 6/26/2024 9:07:45 AM. This article is licensed under a Creative Commons Attribution-NonCommercial 3.0 Unported Licence.

Table 3 Cytotoxic IC_{50} values (μM)[a] and selectivity index[b] of the complexes **2a-Cl**, **2b-PF_6** and **3a-PF_6** in A549, HeLa and BEAS-2B human cell lines compared with cisplatin

	IC50[a]			SI[b]	
Complex	A549	HeLa	BEAS-2B	A549	HeLa
2a-Cl	3.73 ± 0.76	5.53 ± 0.41	12.32 ± 0.21	3.30	2.23
2b-PF_6	27.17 ± 1.44	74.6 ± 0.72	51.6 ± 4.71	1.90	0.69
3a-PF_6	32.87 ± 3.01	51.22 ± 1.29	24.03 ± 3.82	0.73	0.47
Cisplatin	6.45 ± 0.47[c]	13.60 ± 0.99[d]	1.74 ± 0.16	0.27	0.13

[a] IC_{50} values presented as mean ± standard error of the mean of three different experiments. [b] Selectivity index (SI) = IC_{50} nontumor cell (BEAS-2B)/IC_{50} cancer cell (A549 or HeLa), as described in ref. 65, 66. [c] As determined in ref. 67. [d] As determined in ref. 68.

other organometallic complexes with cytotoxic activities toward A549, HeLa, and other cancer cell lines have been previously described,[66,75–78] including iridium organometallic complexes.[18,79,80]

Photoinduced cytotoxicity and intracellular ROS generation. To expand our knowledge on the cytotoxic behaviour of these complexes, we examine their potential as photosensitizers (PS). Selective activation of a nontoxic photosensitizer by light is an attractive regimen for therapy, especially if the PS is preferentially taken up by cancer cells.[81] In recent years, luminescent metal based drugs, in particular Ru(II) Ir(III) and Pt(II) complexes, are being actively investigated due to their outstanding results in PDT based cancer therapy.[40,82–87] Due to the ability of these iridium complexes to generate $^1O_2$ upon irradiation and their photostability, they can be considered as potential tools in phototheranostics. Therefore, we decided to evaluate the potential use of complexes **2b-Cl** and **2c-Cl** in photodynamic therapy based on their light cytotoxic effects in normal cell culture. In addition, we also chose **2b-PF_6** in order to evaluate the effect of changing the counter-anion Cl^- with PF_6^- on the induction of the photocytotoxicity. Finally, we also evaluated the photocytotoxicity of **3a-PF_6** to test the effect of locating the carboxylic units on the diimine ligand. The photostability of the complexes under similar conditions of irradiation to that employed for PDT assays was supported by NMR spectroscopy. A549 cells were initially treated with each complex in Hank's balanced salt solution (HBSS) for 1 h at 37 °C in order to allow cellular interaction and internalization. Then, A549 cells were irradiated with a 396 nm LED lamp located 91 mm apart (5 Mw cm^{-2}) for different times: 3 min (**3a-PF_6**), 10 min (**2b-PF_6**) and 15 min (**2b-Cl** and **2c-Cl**) (see the ESI†). After the irradiation, cells were washed and incubated in complete RPMI medium without the presence of any complex for another 72 hours. Finally, cell viability (IC_{50}) was assessed by the MTS test, as detailed in the ESI.† The observed IC_{50} values were significantly lower in the presence of UV light than under non-UV light, reflecting the effective phototoxicity of the photosensitizers. Thus, as shown in Fig. 8, upon UV light irradiation a significant increase of the antiproliferative activity was observed for **3a-PF_6** (IC_{50}: 5.63 μM) with a short irradiation time of only 3 min. UV-light irradiation for 15 min for **2b-Cl** or 10 min for **2b-PF_6**, also enhances their antiproliferative activity leading to IC_{50} values of 14.39 and 18.57 μM, respectively, whereas the slightly cytotoxic **2c-Cl** showed a lower PI activity, giving a moderate effect by lowering the IC_{50} value to 55.52 μM upon 15 min of irradiation. In any case, the complexes are more active under UV light than under non-UV light. This could be related to their singlet oxygen generation ability in cancer cells. The generation of ROS after UV irradiation was measured using the ROS indicator H2DCFDA. As shown in Table 4, the four complexes show ROS generation after UV irradiation. The highest values were given by **3a-PF_6** (49 μM), which were in good agreement with its lower UV-IC_{50} (Fig. 8d) and despite its shorter UV light exposure time (3 min).

Relative lipophilicity. The relative hydrophobicity of the complexes was studied by RP-UPLC with the aim of establishing a correlation between their cytotoxicity and affinity for a lipid environment, a crucial aspect in their pharmacokinetic properties. Complexes were dissolved in acetonitrile (≈1 ppm), and a mixture of acetonitrile with 0.1% HCOOH (A) and H_2O with 0.1% HCOOH (B) was employed as a mobile phase. The lipophilicity character is based on the values of their retention times (t_R). These values account for the relative interactions between the hydrophobic stationary phase (Aquity UPLC BEH C18) and the hydrophilic mobile phase with each complex. The longer the t_R, the more lipophilic the character of the complex.[62,88] In case of these Ir(III) complexes, the presence of substituents on the cyclometalated groups remarkably decreased the t_R (H > CHO > COOH) (Table S9†), with **2a-Cl** (t_R = 3.28) and **3a-PF_6** (t_R = 1.99) being the most lipophilic ones. The higher lipophilicity of **2a-Cl** is in accordance with the good cytotoxicity activity found for this complex, which displays the lowest IC_{50} values (Table 3). Differences between the t_R of the rest of compounds were too small to ensure a clear relationship between the results and their cytotoxic activities.

Study of the reaction with NADH. Nicotinamide adenine dinucleotide (NADH), and its oxidized form NAD^+, is a coenzyme whose function is crucial for the catalysis of redox or isomerization reactions.[89] NADH plays an important role in the mitochondrial electron transport chain and the maintenance of the cellular redox balance. Thus, any alteration in the intracellular concentration of this species might lead to cell death.[90] Recent studies have reported that some Ir(III) and Os(II) complexes display anticancer activity through a non-conventional redox mediated mechanism of action involving catalytic photo-oxidation of NADH to NAD^+ through transfer hydro-

 This journal is © The Royal Society of Chemistry 2023

Open Access Article. Published on 05 April 2023. Downloaded on 6/26/2024 9:07:45 AM.
This article is licensed under a Creative Commons Attribution-NonCommercial 3.0 Unported Licence.

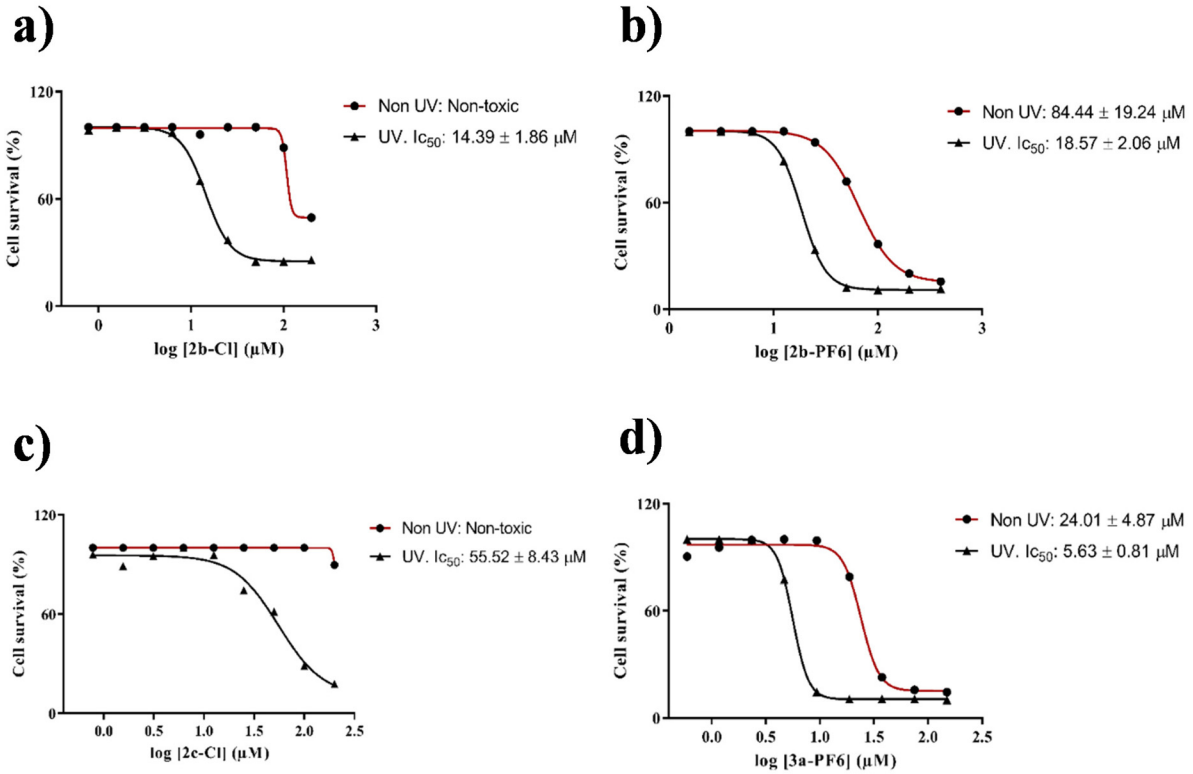

Fig. 8 Dose–response curves for the A549 cell line treated with complex (a) **2b-Cl**; (b) **2b-PF$_6$**; (c) **2c-Cl** and (d) **3a-PF$_6$** either with (triangles) or without (circles) UV light: irradiation with a UV 396 nm LED for 15 min (a and c), 10 min (b) and 3 min (d) and followed by MTS cytotoxic assays performed after 72 h. Non UV-irradiated cells were manipulated identically to UV-irradiated ones. IC_{50} values are presented as mean ± standard error of the mean of three different experiments performed in sextuplicate.

Table 4 ROS production in A549 cell line treated with complexes **2b(Cl and PF$_6$)**, **2c-Cl** and **3a-PF$_6$**, either with or without UV light

Complex		ROS (arbitrary units)[a]	
		Non UV[b]	UV[c]
2b-Cl	Control[d]	801.42 ± 20.00	10 635.50 ± 451.51**
	1 mM	702.67 ± 47.68	46 391.44 ± 818.24***
	25 mM	2976.67 ± 390.74	71 221.42 ± 1906.88***
2b-PF$_6$	Control[d]	516.33 ± 16.78	7527.17 ± 922.78*
	2.5 mM	617.67 ± 24.30	54 776.42 ± 5684.69**
	25 mM	1702.83 ± 61.91	75 723.75 ± 2670.39***
2c-Cl	Control[d]	494.58 ± 34.34	7571.42 ± 1329.36**
	1 mM	468.67 ± 24.83	10 578.25 ± 236.44***
	50 mM	1127.50 ± 118.51	72 319.33 ± 2846.33***
3a-PF$_6$	Control[d]	577.58 ± 71.84	2476.25 ± 130.39***
	1 mM	633.00 ± 32.92	4583.75 ± 92.10***
	7 mM	999.25 ± 37.02	17 801.33 ± 690.25***
	49 mM	1832.75 ± 246.03	82 785.67 ± 1296.15***

[a] ROS was measured using the ROS-sensitive dye, 2′,7′-dichlorodihydrofluorescein diacetate (H2DCFDA) as an indicator. [b] Cells were non-irradiated. [c] Cells were irradiated with a UV 396 nm LED for 15 min (**2b-Cl** and **2c-Cl**), 10 min (**2b-PF$_6$**) and 3 min (**3a-PF$_6$**). [d] ROS values of A549 cells without complex. Each value represents the mean ± standard error from three different experiments performed in quadruplicate. *$p < 0.05$; **$p < 0.01$; ***$p < 0.001$ (Mann–Whitney U test or Student's t-test for comparing two groups).

genation reactions leading to H_2O_2 and reactive oxygen species.[91,92] Thus, the quantification of changes in NADH/NAD^+, is a good method to know if these compounds can produce changes in ROS content by this mechanism. The interaction with NADH was performed with the cytotoxic complex **2a-Cl**, and the results are shown in Fig. 9. The reaction of the complex (1 μM) with NADH (100 μM) dissolved in a solution 20% MeOH in H_2O was monitored by UV-vis at 298 K for 8 hours. Following the continuous decrease with time of the NADH absorption peak at 339 nm, due to its interaction with the complex to give its oxidized form NAD^+,[25,93] allowed us to determine the interaction of NADH (conversion to NAD^+) with the complex. The turnover number (TONs) obtained by the difference between NADH concentration at t_0 and t = 8 hours was 14.0, showing that the NADH had been oxidated to NAD^+. This result indicates that this complex can act as a moderate catalyst for endogenous NADH oxidation. Thus, it could be a mitochondrial target, inducing destabilization of the redox homeostasis and, ultimately, causing apoptosis.

Interaction of complexes with DNA. Knowing their cytotoxic activity, the interaction of iridium **2a-Cl**, **2b-PF$_6$** and **3a-PF$_6$** complexes with DNA was studied by their ability to modify the electrophoretic mobility of the supercoiled covalently closed circular (CCC) and the open circular (OC) forms of pBR322 plasmid DNA (Fig. S23†). To provide a basis for com-

Open Access Article. Published on 05 April 2023. Downloaded on 6/26/2024 9:07:45 AM.
This article is licensed under a Creative Commons Attribution-NonCommercial 3.0 Unported Licence.

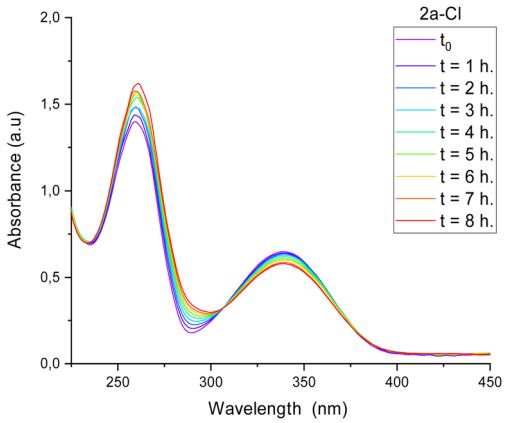

Fig. 9 UV-Vis spectra for the oxidation of NADH (100 μM) by complex **2a-Cl** (1 μM) in a mixture of H_2O/MeOH 80/20 under dark conditions.

parison, the incubation of DNA with cisplatin and the low cytotoxic complex **2c-PF$_6$** was also performed at the same concentrations and conditions. The binding of cisplatin to plasmid DNA, for instance, results in a decrease in the mobility of the CCC form and an increase in the mobility of the OC form (Fig. S23,† upper left panel).[53,66,94,95] As shown in Fig. S23,† no electrophoretic mobility changes were observed after DNA treatment with any complex under the same conditions, thus indicating that these compounds were either not reacting with the DNA or not altering the DNA mobility in agarose gels.

Intracellular localization. Confocal microscopy was performed to investigate the intracellular localization. In agreement with the DNA interaction studies, none of the complexes showed intranuclear localization in A549 cells, as shown in Fig. 10–13. When 16 μM **2a-Cl** complex was incubated with A549 cells, it showed fast cellular internalization, localizing predominantly in lysosomes (Fig. 10), as has been determined by a calculated Pearson correlated coefficient of 0.79. **2a-Cl** also localizes to a lesser extent in the cytoplasm, but not in mitochondria (Fig. S24 and S25†). However, although **2a-Cl** was not detected inside the mitochondria, it ends up causing them damage. Thus, one-hour incubation with 16 μM **2a-Cl** complex induced mitochondrial swelling and the loss of mitochondrial membrane potential was noticed after 30 min (Fig. 11), which has been associated with cell death either by apoptosis or necrosis, depending on the particular biological setting. Accordingly as shown before, this complex effectively alters the NADH/NAD$^+$ pair, which can produce ROS, thus altering mitochondrial functions and cell death.

Complexes **2b-PF$_6$** and **2c-PF$_6$** were also internalized by A549 cells when they were incubated at 32 μM for 1 hour (Fig. 12A and C) or 24 hours (Fig. 12B and D). In agreement with their cytotoxicity results presented in Table 3 and Fig. S22,† the incubation of A549 cells with complex **2b-PF$_6$** for 24 hours resulted in extended cell death while **2c-PF$_6$** complex showed less toxicity for the same time.

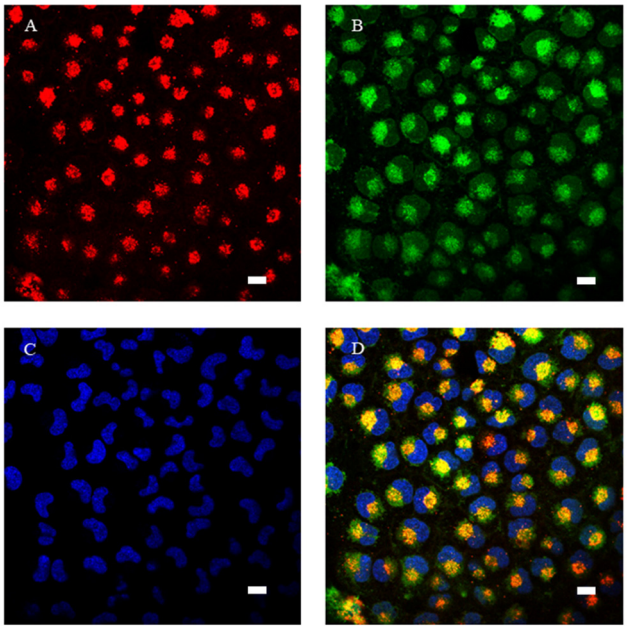

Fig. 10 Laser confocal microscopy images of live A549 cells incubated with 16 μM **2a-Cl** complex for 1 hour. Cells were stained with specific intracellular markers. A. LysoTracker (lysosomal marker, λ_{ex} 543 nm) in red. B. **2a-Cl** (λ_{ex} 405 nm) in green. C. Hoechst (nuclei marker, λ_{ex} 405 nm) in blue. D. Merged image showing colocalization of **2a-Cl** with LysoTracker in lysosomes (yellow). Scale bar = 10 μm.

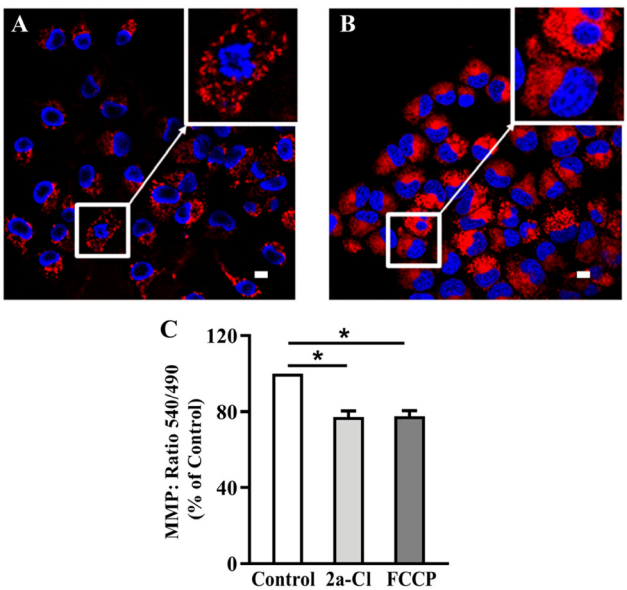

Fig. 11 Laser confocal microscopy images of live A549 cells and loss of mitochondrial membrane potential (MMP) after incubation with **2a-Cl** complex. (A and B) Cells were stained with specific intracellular markers: red: MitoTracker (mitochondrial marker, λ_{ex} 633 nm) and blue: Hoechst (nuclei marker, λ_{ex} 405 nm). (A) Control cells. (B) Cells incubated with 16 μM **2a-Cl** complex for 1 hour. Scale bar = 10 μm. (C) Loss of MMP after 30 min of incubation with 16 μM **2a-Cl** complex or 10 μM FCCP. Control indicates untreated cells. MMP values represent the mean ± standard error from three different experiments performed in quadruplicate. *p < 0.05 (Mann–Whitney U test for comparing two groups).

This journal is © The Royal Society of Chemistry 2023

Open Access Article. Published on 05 April 2023. Downloaded on 6/26/2024 9:07:45 AM.
This article is licensed under a Creative Commons Attribution-NonCommercial 3.0 Unported Licence.

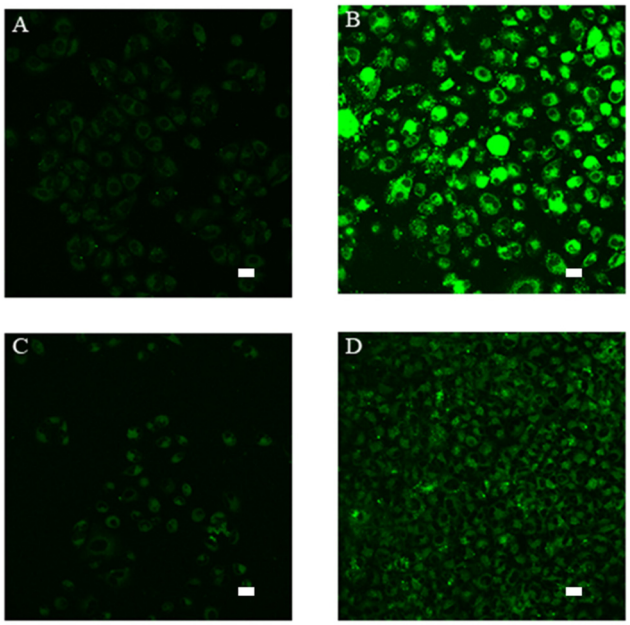

Fig. 12 Laser confocal microscopy images of live A549 cells incubated with 32 μM **2b-PF$_6$** and **2c-PF$_6$** complexes for up to 24 hours. (A) Cells exposed to 32 μM **2b-PF$_6$** for 1 hour (λ_{ex} 405 nm). (B) Cells exposed to 32 μM **2b-PF$_6$** for 24 hours (λ_{ex} 405 nm). (C) Cells exposed to 32 μM **2c-PF$_6$** for 1 hour (λ_{ex} 405 nm). (D) Cells exposed to 32 μM **2c-PF$_6$** for 24 hours (λ_{ex} 405 nm). Scale bar = 20 μm.

Interestingly, when we incubated A549 cells with 45 μM of complex **3a-PF$_6$**, and followed the cells by confocal microscopy, we observed an unexpected behavior. Cells subjected to 405 nm laser stimulation showed increased toxicity compared to adjacent cells not subjected to the laser stimulation (Fig. 13). We did not observe laser-induced toxicity in A549 cells incubated with any of the complexes **2-Cl**. However, 405 nm laser stimulation (from the confocal microscope) not only increased the toxicity of the compound but also increased its fluorescence (central region of pictures in Fig. 13). When we incubated the cells with **3a-PF$_6$** and the mitochondrial marker MitoTracker, we observed loss of mitochondrial membrane potential and mitochondrial swelling (Fig. 13) only when we stimulated the cells with the 405 and the 633 lasers. We found that incubation of cells with **3a-PF$_6$** and MitoTracker and stimulation with 633 nm laser did not damage the mitochondria or induced toxicity. Therefore, we conclude that **3a-PF$_6$** can be excited using 405 nm irradiation increasing its fluorescence and inducing mitochondrial toxicity, possibly by inducing ROS formation (Table 4), leading to cell death. Mitochondria play an important role in many cellular operations, such as the generation of energy, maintaining intracellular redox balance and metabolism and, reports on cyclometalated iridium complexes causing mitochondria mediated dysfunction and apoptosis by several factors including reactive oxygen species (ROS) have been previously reported.[96]

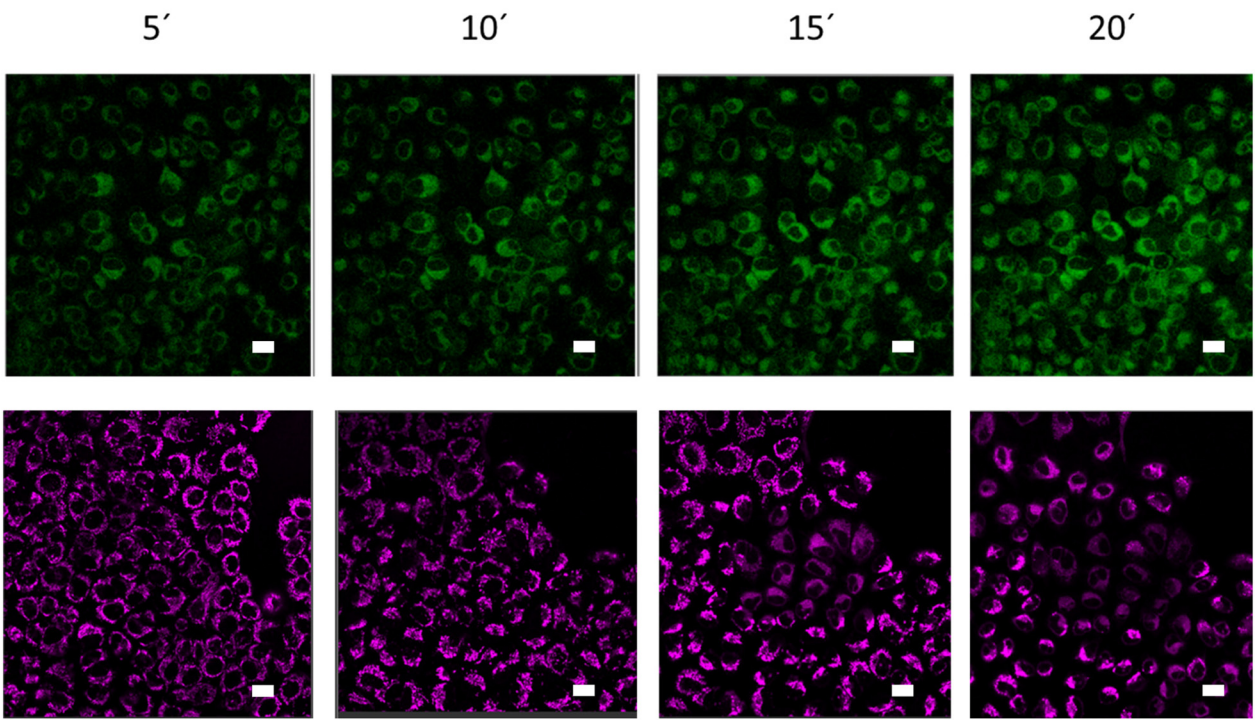

Fig. 13 Laser confocal microscopy images of live A549 cells incubated with 45 μM **3a-PF$_6$** compound for up to 20 minutes. Top pictures: A549 cells incubated with **3a-PF$_6$** stimulated with a 405 nm laser. Bottom pictures: A549 cells incubated with **3a-PF$_6$** and labelled with MitoTracker stimulated with 405 and 633 nm lasers. Green: **3a-PF$_6$**; magenta: MitoTracker. Scale bar = 20 μm.

Open Access Article. Published on 05 April 2023. Downloaded on 6/26/2024 9:07:45 AM.
This article is licensed under a Creative Commons Attribution-NonCommercial 3.0 Unported Licence.

Conclusion

We present here a series of novel Ir(III) cyclometalated cationic complexes incorporating different substituents in the position 3 of the 2,4-diflurophenylpyridinate cyclometalated group (H, dfppy; HCO, CHO-dfppy and COOH, COOH-dfppy) and using *N*,*N*′-dibutyl-2,2′-bipyridine-4,4′-dicarboxamide (*dbbpy*) as the diimine ligand with chloride (**2-Cl**) or PF_6^- ions (**2-PF_6**) as counter anions, together with $[Ir(dfppy)_2(H_2dcbpy)]PF_6$ (**3a-PF_6**), to evaluate the influence of altering the position of the substituents on the optical properties and bioactivity of the complexes. All complexes have been fully characterized by ^1H, $^{13}C\{^1H\}$ and ^{19}F NMR spectroscopy, HMRS, and elemental analysis. In addition, the structure of complex **2a-Cl** and of the cation $[Ir(COOH\text{-}dfppy)_2(dbbpy)]^+$ (from the structure of **2c-PO_2F_2**) were confirmed by X-ray diffraction studies. Crystals of **2a-Cl** reveal that this complex and, likely also complexes **2b,c-Cl**, forms an ionic pair in which the Cl^- establishes strong hydrogen bonding interactions with four H donors of the chelating dbbpy ligand, also supported by an NCI theoretical study. These complexes exhibit bright phosphorescence and a fine tuning of their emission colour can be achieved by modifying the cyclometalated or the substituents of the ancillary diimine ligand. DFT and TD-DFT calculations indicate that all complexes emit from a mixed ^{3}ML′CT (Ir → N^N)/^{3}LL′CT (C^N → N^N) excited state. The complexes can act as $^1O_2$ sensitizers as suggested by the remarkable emission quenching observed in aerated DMSO solutions for all of them and confirmed and calculated in complexes **2b-PF_6** and **3a-PF_6**.

The cytotoxic activity of the new complexes **2** and **3a** has been evaluated against two different human tumour cell lines (A549, lung carcinoma and HeLa, cervix carcinoma) and the nontumoral BEAS-2B (bronchial epithelium) cell line. Only the most lipophilic compound **2a-Cl** has shown remarkable activity in A549 and HeLa cells, significantly better than cisplatin in the same cells. Complexes **2b-PF_6** and **3a-PF_6** exhibited moderate activity, whereas **2b,c-Cl** and **2a-PF_6** did not show cytotoxicity. The binding experiments with the pBR322 plasmid DNA as well as confocal intracellular localization studies revealed that the interaction with nuclear DNA does not seem to be the anticancer mechanism. Complex **2a-Cl** mainly localizes in lysosomes, but it causes mitochondrial damage. Its cytotoxic activity could be in part attributed to the production of ROS generated by intracellular imbalance of the $NADH/NAD^+$ pair, as suggested by the observed oxidation of NADH in the presence of complex **2a-Cl**.

Moreover, these complexes were photo-cytotoxic agents. Thus, a significant increase of antiproliferative activity was observed for complexes **2b-Cl** and **2b-PF_6**, and, particularly, for **3a-PF_6**, upon short irradiation times, which has been related to their singlet oxygen generation ability in cancer cells.

Conflicts of interest

There are no conflicts to declare.

Acknowledgements

This work was supported by the Spanish Ministerio de Ciencia e Innovación (Project PID2019-109742GB-I00) funded by MCIN/AIE/10.13039/501100011033, by "ERDF A way of making Europe", by the "European Union, and by the ADER (Gobierno de La Rioja; Project 2017-I-IDD-00031). G. M. is grateful to UR for a PhD grant. We are grateful to E. Alfaro-Arnedo for her technical help.

References

1 M. Fanelli, M. Formica, V. Fusi, L. Giorgi, M. Micheloni and P. Paoli, *Coord. Chem. Rev.*, 2016, **310**, 41.
2 V. Brabec, O. Hrabina and J. Kasparkova, *Coord. Chem. Rev.*, 2017, **351**, 2.
3 B. J. Pages, K. B. Garbutcheon-Singh and J. R. Aldrich-Wright, *Eur. J. Inorg. Chem.*, 2017, 1613.
4 N. J. Wheate, S. Walker, G. E. Craig and R. Oun, *Dalton Trans.*, 2010, **39**, 8113.
5 W.-P. To, T. Zou, R. W.-Y. Sun and C.-M. Che, *Philos. Trans. R. Soc., A*, 2013, **371**, 20120126.
6 T. C. Johnstone, K. Suntharalingam and S. J. Lippard, *Chem. Rev.*, 2016, **116**, 3436.
7 X. Wang, X. Wang and Z. Guo, *Acc. Chem. Res.*, 2015, **48**, 2622.
8 Q. Cheng and Y. Liu, *Wiley Interdiscip. Rev.: Nanomed. Nanobiotechnol.*, 2017, **9**, e1410.
9 L. G. Marcu, *Pharmaceuticals*, 2022, **15**, 255.
10 S. A. Aldossary, *Biomed. Pharmacol. J.*, 2019, **12**, 7.
11 A. Khoury, K. M. Deo and J. R. Aldrich-Wright, *J. Inorg. Biochem.*, 2020, **207**, 111070.
12 C. Yu, Z. Wang, Z. Sun, L. Zhang, W. Zhang, Y. Xu and J.-J. Zhang, *J. Med. Chem.*, 2020, **63**, 13397.
13 E. Ortega, G. Vigueras, F. J. Ballester and J. Ruiz, *Coord. Chem. Rev.*, 2021, **446**, 214129.
14 L. Feng, M. Gao, D. Tao, Q. Chen, H. Wang, Z. Dong, M. Chen and Z. Liu, *Adv. Funct. Mater.*, 2016, **26**, 2207.
15 L. He, K. Xiong, L. Wang, R. Guan, Y. Chen, L. Ji and H. Chao, *Chem. Commun.*, 2021, **57**, 8308.
16 P.-Y. Ho, C.-L. Ho and W.-Y. Wong, *Coord. Chem. Rev.*, 2020, **413**, 213267.
17 Z. Yang, G. Jiang, Z. Xu, S. Zhao and W. Liu, *Coord. Chem. Rev.*, 2020, **423**, 213492.
18 U. Das, B. Kar, S. Pete and P. Paira, *Dalton Trans.*, 2021, **50**, 11259.
19 N. Nayeem and M. Contel, *Eur. J. Chem.*, 2021, **27**, 8891.
20 P. Sudhindra, S. A. Sharma, N. Roy, P. Moharana and P. Paira, *Polyhedron*, 2020, **192**, 114827.
21 C. C. Konkankit, S. C. Marker, K. M. Knopf and J. J. Wilson, *Dalton Trans.*, 2018, **47**, 9934.
22 Y. Liu, Y. Wang, S. Song and H. Zhang, *Chem. Sci.*, 2021, **12**, 12234.
23 S. Pete, N. Roy and P. Paira, *Inorg. Chim. Acta*, 2021, **517**, 120184.

This journal is © The Royal Society of Chemistry 2023

Open Access Article. Published on 05 April 2023. Downloaded on 6/26/2024 9:07:45 AM.
This article is licensed under a Creative Commons Attribution-NonCommercial 3.0 Unported Licence.

24 G.-X. Xu, E. C.-L. Mak and K. K.-W. Lo, *Inorg. Chem. Front.*, 2021, **8**, 4553.
25 E. Zafon, I. Echevarría, S. Barrabés, B. R. Manzano, F. A. Jalón, A. M. Rodríguez, A. Massaguer and G. Espino, *Dalton Trans.*, 2022, **51**, 111.
26 A. Bonfiglio, C. McCartin, U. Carrillo, C. Cebrian, P. C. Gros, S. Fournel, A. Kichler, C. Daniel and M. Mauro, *Eur. J. Inorg. Chem.*, 2021, **2021**, 1551.
27 Z. Liu and P. J. Sadler, *Acc. Chem. Res.*, 2014, **47**, 1174.
28 X.-D. Song, X. Kong, S.-F. He, J.-X. Chen, J. Sun, B.-B. Chen, J.-W. Zhao and Z.-W. Mao, *Eur. J. Med. Chem.*, 2017, **138**, 246.
29 G. Li, H. Liu, R. Feng, T.-S. Kang, W. Wang, C.-N. Ko, C.-Y. Wong, M. Ye, D.-L. Ma, J.-B. Wan and C.-H. Leung, *Redox Biol.*, 2021, **48**, 102129.
30 W.-Y. Zhang, F. Du, M. He, L. Bai, Y.-Y. Gu, L.-L. Yang and Y.-J. Liu, *Eur. J. Med. Chem.*, 2019, **178**, 390.
31 M.-M. Wang, X.-L. Xue, X.-X. Sheng, Y. Su, Y.-Q. Kong, Y. Qian, J.-C. Bao, Z. Su and H.-K. Liu, *RSC Adv.*, 2020, **10**, 5392.
32 B.-B. Chen, N.-L. Pan, J.-X. Liao, M.-Y. Huang, D.-C. Jiang, J.-J. Wang, H.-J. Qiu, J.-X. Chen, L. Li and J. Sun, *J. Inorg. Biochem.*, 2021, **219**, 111450.
33 N. Roy, U. Sen, S. R. Chaudhuri, V. Muthukumar, P. Moharana, P. Paira, B. Bose, A. Gauthaman and A. Moorthy, *Dalton Trans.*, 2021, **50**, 2268.
34 S. Shaikh, Y. Wang, F. ur Rehman, H. Jiang and X. Wang, *Coord. Chem. Rev.*, 2020, **416**, 213344.
35 X. Liu, K. Li, L. Shi, H. Zhang, Y.-H. Liu, H.-Y. Wang, N. Wang and X.-Q. Yu, *Chem. Commun.*, 2021, **57**, 2265.
36 P. K.-K. Leung, L. C.-C. Lee, H. H.-Y. Yeung, K.-W. Io and K. K.-W. Lo, *Chem. Commun.*, 2021, **57**, 4914.
37 J. Hao, H. Zhang, L. Tian, L. Yang, Y. Zhou, Y. Zhang, Y. Liu and D. Xing, *J. Inorg. Biochem.*, 2021, **221**, 111465.
38 S. Lee and W.-S. Han, *Inorg. Chem. Front.*, 2020, **7**, 2396.
39 A. F. Henwood and E. Zysman-Colman, *Chem. Commun.*, 2017, **53**, 807.
40 H. Huang, S. Banerjee and P. J. Sadler, *ChemBioChem*, 2018, **19**, 1574.
41 M. R. Schreier, X. Guo, B. R. Pfund, Y. Okamoto, T. R. Ward, C. Kerzig and O. S. Wenger, *Acc. Chem. Res.*, 2022, **55**, 1290.
42 N. Okamura, T. Nakamura, S. Yagi, T. Maeda, H. Nakazumi, H. Fujiwara and S. Koseki, *RSC Adv.*, 2016, **6**, 51435.
43 A. Kimyonok, B. Domercq, A. Haldi, J.-Y. Cho, J. R. Carlise, X.-Y. Wang, L. E. Hayden, S. C. Jones, S. Barlow, S. R. Marder, B. Kippelen and M. Weck, *Chem. Mater.*, 2007, **19**, 5602.
44 C. Sahin, A. Goren, S. Demir and M. S. Cavus, *New J. Chem.*, 2018, **42**, 2979.
45 F. Lafolet, S. Welter, Z. Popović and L. De Cola, *J. Mater. Chem.*, 2005, **15**, 2820.
46 Y. Zhou, W. Li, Y. Liu and M. Zhou, *ChemPlusChem*, 2013, **78**, 413.
47 J. B. Waern, C. Desmarets, L.-M. Chamoreau, H. Amouri, A. Barbieri, C. Sabatini, B. Ventura and F. Barigelletti, *Inorg. Chem.*, 2008, **47**, 3340.
48 S. Bettington, M. Tavasli, M. R. Bryce, A. S. Batsanov, A. L. Thompson, H. A. Al Attar, F. B. Dias and A. P. Monkman, *J. Mater. Chem.*, 2006, **16**, 1046.
49 C. Lorenzo-Aparicio, M. G. Gallego, C. R. de Arellano and M. A. Sierra, *Dalton Trans.*, 2022, **51**, 5138.
50 B. Orwat, M. J. Oh, M. Zaranek, M. Kubicki, R. Januszewski and I. Kownacki, *Inorg. Chem.*, 2020, **59**, 9163.
51 E. Martìnez-Vollbert, C. Ciambrone, W. Lafargue-Dit-Hauret, C. Latouche, F. Loiseau and P.-H. Lanoë, *Inorg. Chem.*, 2022, **61**, 3033.
52 S. A. Fitzgerald, H. Y. Otaif, Christopher E. Elgar, N. Sawicka, P. N. Horton, S. J. Coles, J. M. Beames and S. J. A. Pope, *Inorg. Chem.*, 2021, **60**, 15467–15484.
53 M. Martínez-Junquera, E. Lalinde, M. T. Moreno, E. Alfaro-Arnedo, I. P. López, I. M. Larráyoz and J. G. Pichel, *Dalton Trans.*, 2021, **50**, 4539.
54 M. Martínez-Alonso, P. Sanz, P. Ortega, G. Espino, F. A. Jalon, M. Martin, A. M. Rodríguez, J. A. Lopez, C. Tejel and B. R. Manzano, *Inorg. Chem.*, 2020, **59**, 14171.
55 V. Nemec, K. Lisac, N. Bedeković, L. Fotović, V. Stilinović and D. J. C. Cinčić, *CrystEngComm*, 2021, **23**, 3063.
56 G. R. Desiraju, *Acc. Chem. Res.*, 2002, **35**, 565.
57 S. Bhattacharjee and S. Bhattacharya, *Chem. Commun.*, 2015, **51**, 7019.
58 L. M. Cavinato, G. Millán, J. Fernández-Cestau, E. Fresta, E. Lalinde, J. R. Berenguer and R. D. Costa, *Adv. Funct. Mater.*, 2022, 2201975.
59 M. Rico-Santacruz, Á. E. Sepúlveda, C. Ezquerro, E. Serrano, E. Lalinde, J. R. Berenguer and J. García-Martínez, *Appl. Catal., B*, 2017, **200**, 93.
60 I. Echevarría, E. Zafon, S. Barrabés, M. Á. Martínez, S. Ramos-Gómez, N. Ortega, B. R. Manzano, F. A. Jalón, R. Quesada and G. Espino, *J. Inorg. Biochem.*, 2022, **231**, 111790.
61 R. D. Costa, E. Orti, H. J. Bolink, F. Monti, G. Accorsi and N. Armaroli, *Angew. Chem., Int. Ed.*, 2012, **51**, 8178.
62 R. Lara, G. Millan, M. T. Moreno, E. Lalinde, E. Alfaro-Arnedo, I. P. Lopez, I. M. Larrayoz and J. G. Pichel, *Chem. – Eur. J.*, 2021, **27**, 15757.
63 R. H. Young, K. Wehrly and R. L. Martin, *J. Am. Chem. Soc.*, 1971, **93**, 5774.
64 Y. Lu, R. Conway-Kenny, J. Wang, X. Cui, J. Zhao and S. M. Draper, *Dalton Trans.*, 2018, **47**, 8585.
65 O. A. Peña-Morán, M. L. Villarreal, L. Álvarez-Berber, A. Meneses-Acosta and V. Rodríguez-López, *Molecules*, 2016, **21**, 1013.
66 G. Millan, N. Gimenez, R. Lara, J. R. Berenguer, M. T. Moreno, E. Lalinde, E. Alfaro-Arnedo, I. P. Lopez, S. Pineiro-Hermida and J. G. Pichel, *Inorg. Chem.*, 2019, **58**, 1657.
67 J. R. Berenguer, J. G. Pichel, N. Gimenez, E. Lalinde, M. T. Moreno and S. Pineiro-Hermida, *Dalton Trans.*, 2015, **44**, 18839.
68 E. Lalinde, R. Lara, I. P. Lopez, M. T. Moreno, E. Alfaro-Arnedo, J. G. Pichel and S. Pineiro-Hermida, *Chem. – Eur. J.*, 2018, **24**, 2440.

Open Access Article. Published on 05 April 2023. Downloaded on 6/26/2024 9:07:45 AM.
This article is licensed under a Creative Commons Attribution-NonCommercial 3.0 Unported Licence.

69 F.-X. Wang, M.-H. Chen, X.-Y. Hu, R.-R. Ye, C.-P. Tan, L.-N. Ji and Z.-W. Mao, *Sci. Rep.*, 2016, **6**, 38954.
70 R. B. Badisa, S. F. Darling-Reed, P. Joseph, J. S. Cooperwood, L. M. Latinwo and C. B. Goodman, *Anticancer Res.*, 2009, **29**, 2993.
71 J. A. Valderrama, V. Delgado, S. Sepúlveda, J. Benites, C. Theoduloz, P. Buc Calderon and G. G. Muccioli, *Molecules*, 2016, **21**, 1199.
72 G. I. Davou, N. Chuwang, U. Essien, T. Choji, B. Echeonwu and M. Lugos, *Int. Res. J. Med. Med. Sci.*, 2019, **7**, 40.
73 J. Chen, J. Wang, Y. Deng, T. Wang, T. Miao, C. Li, X. Cai, Y. Liu, J. Henri and L. Chen, *Bioinorg. Chem. Appl.*, 2020, **2020**, 8890950.
74 M. S. Costa, Y. G. Gonçalves, B. C. Borges, M. J. B. Silva, M. K. Amstalden, T. R. Costa, L. M. G. Antunes, R. S. Rodrigues, V. D. M. Rodrigues, E. de Faria Franca, M. A. P. Zoia, T. G.de Araújo, L. R. Goulart, G. Von Poelhsitz and K. A. G. Yoneyama, *Sci. Rep.*, 2020, **10**, 15410.
75 C. Li, K.-W. Ip, W.-L. Man, D. Song, M.-L. He, S.-M. Yiu, T.-C. Lau and G. Zhu, *Chem. Sci.*, 2017, **8**, 6865.
76 E. Petruzzella, R. Sirota, I. Solazzo, V. Gandin and D. Gibson, *Chem. Sci.*, 2018, **9**, 4299.
77 P. Wiji Prasetyaningrum, A. Bahtiar and H. Hayun, *Sci. Pharm.*, 2018, **86**, 25.
78 N. Pantelić, B. B. Zmejkovski, D. D. Marković, J. M. Vujić, T. P. Stanojković, T. J. Sabo and G. N. Kaluđerović, *Metals*, 2016, **6**, 226.
79 A. Zamora, G. Vigueras, V. Rodríguez, M. D. Santana and J. Ruiz, *Coord. Chem. Rev.*, 2018, **360**, 34.
80 C. Caporale and M. Massi, *Coord. Chem. Rev.*, 2018, **363**, 71.
81 T. C. Pham, V.-N. Nguyen, Y. Choi, S. Lee and J. Yoon, *Chem. Rev.*, 2021, **121**, 13454.
82 B. Kar, U. Das, N. Roy and P. Paira, *Coord. Chem. Rev.*, 2023, **474**, 214860.
83 D. Wei, Y. Huang, B. Wang, L. Ma, J. Karges and H. Xiao, *Angew. Chem., Int. Ed.*, 2022, **61**, e202201486.
84 G. De Soricellis, F. Fagnani, A. Colombo, C. Dragonetti and D. Roberto, *Inorg. Chim. Acta*, 2022, **541**, 121082.
85 R. Guan, L. Xie, L. Ji and H. Chao, *Eur. J. Inorg. Chem.*, 2020, **2020**, 3978.
86 D. Ashen-Garry and M. Selke, *Photochem. Photobiol.*, 2014, **90**, 257.
87 Y. Wu, S. Li, Y. Chen, W. He and Z. Guo, *Chem. Sci.*, 2022, **13**, 5085.
88 J. Yellol, S. A. Perez, A. Buceta, G. Yellol, A. Donaire, P. Szumlas, P. J. Bednarski, G. Makhloufi, C. Janiak and A. Espinosa, *J. Med. Chem.*, 2015, **58**, 7310.
89 Z. Liu, I. Romero-Canelón, B. Qamar, J. M. Hearn, A. Habtemariam, N. P. Barry, A. M. Pizarro, G. J. Clarkson and P. J. Sadler, *Angew. Chem.*, 2014, **126**, 4022.
90 H. Huang, S. Banerjee, K. Qiu, P. Zhang, O. Blacque, T. Malcomson, M. J. Paterson, G. J. Clarkson, M. Staniforth and V. G. Stavros, *Nat. Chem.*, 2019, **11**, 1041.
91 C. Huang, C. Liang, T. Sadhukhan, S. Banerjee, Z. Fan, T. Li, Z. Zhu, P. Zhang, K. Raghavachari and H. Huang, *Angew. Chem.*, 2021, **133**, 9560.
92 Z. Fan, J. Xie, T. Sadhukhan, C. Liang, C. Huang, W. Li, T. Li, P. Zhang, S. Banerjee and K. Raghavachari, *Chem. – Eur. J.*, 2022, **28**, e202103346.
93 X. Liu, X. He, X. Zhang, Y. Wang, J. Liu, X. Hao, Y. Zhang, X. A. Yuan, L. Tian and Z. Liu, *ChemBioChem*, 2019, **20**, 2767.
94 M. Frik, J. Jiménez, V. Vasilevski, M. Carreira, A. De Almeida, E. Gascón, F. Benoit, M. Sanaú, A. Casini and M. Contel, *Inorg. Chem. Front.*, 2014, **1**, 231.
95 G. L. Cohen, W. R. Bauer, J. K. Barton and S. J. Lippard, *Science*, 1979, **203**, 1014.
96 R. L. Panchangam, R. N. Rao, M. M. Balamurali, T. B. Hingamire, D. Shanmugam, V. Manickam and K. Chanda, *Inorg. Chem.*, 2021, **60**, 17593.

This journal is © The Royal Society of Chemistry 2023